

Creation of Electron–Positron Wind in Gamma-Ray Bursts and Its Effect on the Early Afterglow Emission

P. Kumar¹ and A. Panaitescu²

¹*Astronomy Department, University of Texas, Austin, TX 78731, e-mail: pk@astro.as.utexas.edu*

²*Dept. of Astrophysical Sciences, Princeton University, Princeton, NJ 08544, e-mail: adp@astro.princeton.edu*

24 November 2018

ABSTRACT

We calculate the creation of electron–positron pairs in Gamma-Ray Bursts (GRBs) resulting from the collision between scattered and outward moving gamma-ray photons. The number of pairs exceeds the number of ambient medium electrons encountered by the GRB ejecta up to $\sim 10^{16}$ cm from the center of explosion. The shock resulting from the interaction of the ejecta with the pair-wind may brighten the afterglow synchrotron emission during the first few minutes. Even without this effect, the peak intensity of the optical afterglow increases with the density of the surrounding medium. Therefore, observations of the optical flux at early times constrain the density of the circumburst medium. If the electron and magnetic field energies behind the forward shock sweeping-up the pair-wind and the circumburst medium are as inferred from fits to the broadband afterglow emission at 0.5 – 100 days, then the current upper limits on the optical counterpart emission, set by the ROTSE and LOTIS experiments, indicate that the circumburst medium within 0.01 pc is less dense than 100 cm^{-3} or, if a wind, corresponds to a progenitor mass-loss to wind speed ratio below $10^{-6} M_{\odot}/\text{yr}/(10^3 \text{ km/s})$.

Key words: radiation mechanisms: non-thermal – relativity – shock waves – gamma-rays: bursts, theory

1 INTRODUCTION

The γ -photons produced in Gamma-Ray Bursts (GRBs) are scattered by electrons in the medium surrounding the explosion, their interaction with the outward moving photons creates an electron and positron pair if the photons energy in their center of mass frame exceeds $2m_e c^2$. These pairs scatter more photons, leading to an exponential growth of their density. The pairs are accelerated by scattering the gamma-ray burst photons.

The process of pair-creation in GRBs has been previously considered by Thompson & Madau (2000), Mészáros, Ramirez-Ruiz & Rees (2001), and Beloborodov (2002). The resulting pair-wind moves at a relativistic velocity and the pairs dominate the number density of charged particles up to a distance $10^{16} (E_{\gamma}/10^{53})^{1/2}$ cm from the center of explosion, where E_{γ} is the isotropic-equivalent GRB energy release. The purpose of this paper is to consider the effect of pairs created by GRB pulse on early afterglow emission.

In §2 we consider all of previously discussed physical processes for electron-positron pair creation by GRB photons. We include in our calculations the overtaking of pair plasma by the material ejected in the explosion, which can

substantially reduce the number of pairs produced. In §3 we consider the effect of pairs on early afterglow emission, and calculate for various external densities and ejecta Lorentz factor the optical synchrotron emission produced by the shock that heats up the pair-wind when it collides with the GRB ejecta. The non-detection of early optical afterglow emission brighter than magnitude $R \sim 13$ by the ROTSE and LOTIS experiments can be used to provide an upper limit on the density of the circumburst medium.

2 DYNAMICS OF THE ELECTRON–POSITRON WIND

The e^{\pm} enrichment is calculated from the energy spectrum of the incident and scattered photons. We approximate the GRB energy spectrum as a power-law $F(\varepsilon) = F_p(\varepsilon/\varepsilon_p)^{-\alpha}$ for $\varepsilon > \varepsilon_p$. For most of the 5,500 spectra of the 156 bright BATSE bursts analyzed by Preece et al. (2000), the spectral slope α above the ε_p break is between 0.5 and 2.5, with the peak of the distribution at 1.3, while ε_p is between 70 keV and 800 keV, its distribution peaking at 250 keV. Assuming a burst redshift $z = 1$, the corrected break energy ε_p ,

measured in $m_e c^2$ units is between 0.3 and 3, with a peak at 1.

The flux of scattered photons at some distance x from the leading edge of the gamma-ray pulse, is calculated numerically by integrating over the scatterings that occurred from $x = 0$ to the current x and over the primary photon spectrum and deflection angle, taking into account the photon attenuation during its propagation.

2.1 Planar Geometry

In planar geometry, the laboratory frame number density n_{\pm} of the created pairs and their streaming velocity βc are given by

$$\frac{d}{dx} [n_{\pm}(1 - \beta)] = 2 \frac{dn_{\pm}}{dt}, \quad (1)$$

$$\frac{d}{dx} \{ [2n_{\pm} m_e + n_p(m_e + m_p)] \gamma \beta (1 - \beta) c^2 \} = \frac{dP_{sc}}{dt} + \frac{dP_{\pm}}{dt}, \quad (2)$$

respectively, where t is time measured in the laboratory frame, n_p is the laboratory frame number density of the swept-up external medium electrons, m_p is the proton mass, and γ is the pair-wind Lorentz factor. The right-hand side of equation (1) represents the rate of pair creation from scattered and primary photons, while the two terms in the rhs of equation (2) represent the rate of momentum deposition by pair formation and by photon scattering, respectively. Conservation of the number of external electrons implies that

$$\frac{d}{dx} [n_p(1 - \beta)] = 0, \quad (3)$$

i.e. $n_p = n/(1 - \beta)$, n being the density of the unperturbed circumburst medium.

The most general form of the rhs's of equations (1) and (2) are given by Beloborodov (2002) (see his equations [10] and [16]). For analytical purposes we simplify them by making two approximations. First, we ignore the angular dependence of the photon scattering probability and consider that an electron (or positron) at x deflects an incident photon only by the average deflection angle $\cos^{-1} \beta(x)$. This approximation reduces the integral of the scattered flux from one over the wind volume to one over a surface from which scattered photons arrive at the same time at x (where e^{\pm} creation takes place). Secondly, we consider that the e^{\pm} pairs are produced mostly by photons near the peak of the spectrum, i.e. in the integral over the spectrum of primary photons we approximate by unity the term $1 + \varepsilon/\gamma$, where ε is the photon energy in $m_e c^2$ units. This approximation is justified by that photons with $\varepsilon > \gamma$ are scattered in the Klein-Nishina regime, thus the scattering probability is reduced. Taking into account that the GRB photon spectrum above $m_e c^2$ is typically steeper than ε^{-2} , the latter approximation is more suitable at locations x where the wind is relativistic ($\gamma \gg 1$).

With the above approximations, equation (1) for the wind number density becomes

$$\frac{d}{dx} [\tilde{n}(1 - \beta)] = \frac{2^{-\alpha+1} \phi(\alpha)}{\lambda^2} \int_0^x dx' \tilde{n}(x') \frac{1 - \beta(x')}{1 + \beta(x')} \times$$

$$\int_{\varepsilon_p}^{\varepsilon_{kn}(x')} \frac{d\varepsilon}{\varepsilon} f(\varepsilon) f(\varepsilon_t), \quad f(\varepsilon) = \left(\frac{\varepsilon}{\varepsilon_p} \right)^{-\alpha}, \quad (4)$$

where $\tilde{n} = 2n_{\pm} + n_p$ is the total lepton density, and $\phi(\alpha) \simeq (7/12)(1 + \alpha)^{-5/3}$ (Svensson 1987),

$$\lambda = \frac{c}{F_p \sigma_T}, \quad (5)$$

σ_T being the Thomson scattering cross-section, and

$$\varepsilon_t = \frac{2(1 + \beta)}{\varepsilon(1 - \beta)}, \quad \varepsilon_{kn} \simeq \gamma(1 + \beta), \quad (6)$$

are the photon threshold energy for e^{\pm} formation and the Klein-Nishina ‘‘cut-off’’ photon energy, respectively. Note that for $\varepsilon_p < 2$ (i.e. the peak of the GRB νF_{ν} spectrum is below ~ 1 MeV), ε_t is larger than ε_p .

With the same approximations, equation (2) for the wind momentum density becomes:

$$\begin{aligned} \frac{d}{dx} \left[\left(\tilde{n} + \frac{m_p}{m_e} n_p \right) \gamma \beta (1 - \beta) \right] &= \frac{\tilde{n}(1 - \beta)}{\lambda(1 + \beta)} \int_{\varepsilon_p}^{\varepsilon_{kn}(x)} d\varepsilon f(\varepsilon) \\ &+ \frac{\phi(\alpha)}{\lambda^2} \int_0^x dx' \tilde{n}(x') \frac{1 - \beta'}{1 + \beta'} \int_{\varepsilon_p}^{\varepsilon_{kn}(x')} \frac{d\varepsilon}{\varepsilon} f(\varepsilon) f(\varepsilon_t) p_{\pm}, \end{aligned} \quad (7)$$

where

$$p_{\pm} = \frac{\varepsilon \beta'}{1 + \beta'} + \frac{\phi(\alpha - 1)}{\varepsilon \phi(\alpha)} \frac{1 + \beta'}{1 - \beta'}, \quad \beta' \equiv \beta(x'), \quad (8)$$

is the total radial momentum of the scattered and primary photons that form a e^{\pm} pair. Equations (4)-(7) are similar to equations (42)-(47) of Beloborodov (2002).

For a power-law photon spectrum, equation (4) leads to

$$\frac{d}{dx} [\tilde{n}(1 - \beta)] = \frac{\phi(\alpha)}{2^{\alpha-1}} \frac{\varepsilon_p^{2\alpha}}{\lambda^2} \int_0^x dx' \tilde{n}(x') \frac{\ln(\varepsilon_{kn}/\varepsilon_p)}{[(1 + \beta')\gamma']^{2\alpha+2}}. \quad (9)$$

The integrand in the above equation decreases rapidly with γ , most of the contribution to the integral coming from $\gamma \lesssim 2$. Physically, this means that pairs are created by photons scattered by mildly or non-relativistic pairs; the e^{\pm} threshold for photons scattered by relativistic e^{\pm} is much greater because these photons are moving within an angle γ^{-1} relative to the primary photons.

As shown in Beloborodov (2002) the momentum deposition in the e^{\pm} wind through pair creation is at most comparable to that transferred by photon scattering. For simplicity, we retain only the scattering term in equation (7), reducing it to

$$\frac{d}{dx} \left[\frac{(\tilde{n} m_e + n_p m_p) \beta}{\gamma(1 + \beta)} \right] = \frac{m_e \varepsilon_p}{(\alpha - 1) \lambda} \frac{\tilde{n}}{(1 + \beta)^2 \gamma^2}. \quad (10)$$

2.1.1 Non-Relativistic Wind

In the $\beta \ll 1$ limit, equations (9) and (10) lead to an exponential growth of the pair density and velocity:

$$\tilde{n}(x) = n e^{x/x_{\pm}}, \quad \beta(x) = \frac{\varepsilon_p}{(\alpha - 1) m_p} \frac{m_e}{\lambda} x_{\pm} e^{x/x_{\pm}}, \quad (11)$$

for $x > x_{\pm}$, where

$$x_{\pm} = \sqrt{\frac{2^{\alpha-1}}{\phi(\alpha)} \frac{\lambda}{\varepsilon_p^{\alpha}}} \stackrel{\alpha=1.5}{\approx} 3 \varepsilon_p^{-3/2} \lambda, \quad (12)$$

is the length-scale for pair loading. For a GRB of isotropic-equivalent output energy E_{γ} , equation (5) gives for the acceleration length-scale at radius r

$$\frac{x_{\pm}}{\Delta} = \frac{\pi}{\alpha - 1} \sqrt{\frac{2^{\alpha+3}}{\phi(\alpha)} \frac{m_e c^2}{\sigma_T} \frac{r^2}{\varepsilon_p^{\alpha-1} E_{\gamma}}} \stackrel{\alpha=1.5}{\approx} 0.1 \frac{r_{16}^2}{E_{\gamma,53} \varepsilon_p^{1/2}}, \quad (13)$$

where $\Delta = cT/(1+z)$ is the geometrical thickness of the GRB front, T being the observed burst duration, z the GRB's redshift, and the usual scaling $X_n = X/10^n$ was used.

From equation (11) we see that the wind acceleration length-scale x_{acc} , defined by $\gamma(x_{acc}) = 2$ is a factor of a few larger than x_{\pm} . A simple estimate of x_{acc} can be obtained by equating the momentum deposited by photon scattering $\tilde{n}_{acc}(\sigma_T x_{acc})(F_p \varepsilon_p m_e c^2 / c^2) = \tilde{n}_{acc} \varepsilon_p (m_e c)(x_{acc} / \lambda)$ (considering that all photons have the same energy $m_e c^2 \varepsilon_p$) with the momentum $(\tilde{n}_{acc} m_e + n_{p,acc} m_p) c \sim n m_p c$ of the medium (assuming that the wind mass density is dominated by the protons, i.e. $\tilde{n}(x_{acc}) \ll n_p(x_{acc})(m_p/m_e)$, and that $n_p(x_{acc}) \approx n$):

$$\frac{x_{acc}}{\lambda} e^{x_{acc}/x_{\pm}} = \frac{m_p}{m_e \varepsilon_p^2} \rightarrow x_{acc} \stackrel{\varepsilon_p=1}{\approx} 5 x_{\pm}. \quad (14)$$

Then equation (13) shows that the wind is accelerated to a relativistic speed for radii smaller than

$$r_{end} \stackrel{\alpha=1.5}{\sim} 10^{16} \varepsilon_p^{1/4} E_{\gamma,53}^{1/2} \text{ cm}. \quad (15)$$

2.1.2 Relativistic Wind

For $x \gg x_{acc}$ we can solve the pair density and momentum equations together to obtain $\tilde{n}(x)$ & $\gamma(x)$. We consider a power-law solution of the form

$$\tilde{n}(x) = A_1 \left(\frac{x}{x_{acc}} \right)^{a_1}, \quad \gamma(x) = \frac{A_2}{2} \left(\frac{x}{x_{acc}} \right)^{a_2}. \quad (16)$$

Substituting this into equations (9) and (10), and assuming that the mass density is dominated by protons i.e., the number of pairs per proton is much less than m_p/m_e , we obtain

$$(a_1 - 2a_2) A_2^{2\alpha} y^{a_1 - 2a_2 - 1} = 2\eta^2 \int_{x_{min}}^x \frac{dx'}{x_{acc}} y'^{a_1 - 2(\alpha+1)a_2}, \quad (17)$$

$$\frac{a_2 n m_p y^{a_2 - 1}}{x_{acc}} = \frac{m_e \varepsilon_p}{\lambda(\alpha - 1)} \left(\frac{A_1}{A_2^3} \right) y^{a_1 - 2a_2}, \quad (18)$$

where $y \equiv x/x_{acc}$, $\eta \equiv x_{acc}/x_{\pm}$ is a constant independent of x , and x_{min} is determined by the condition that the pair creation optical depth for a photon scattered at x_{min} , of energy $\sim \varepsilon_p$, is unity between x_{min} and x ; x_{min} is determined by the following equation

$$\tau_{\gamma\gamma} \approx (x - x_{min}) \frac{\sigma_T f(\varepsilon_t)}{m_e c^3} \approx 1, \quad \varepsilon_t \approx \frac{2(1+\beta)}{\varepsilon_p(1-\beta)} \approx \frac{8\gamma^2}{\varepsilon_p}. \quad (19)$$

By substituting (16) in the above equation we find x_{min} explicitly

$$\tau_{\gamma\gamma} \approx \frac{x - x_{min}}{2\alpha\lambda} \left(\frac{\varepsilon_p}{2\gamma} \right)^{2\alpha} \approx \frac{x \varepsilon_p^{2\alpha}}{2\alpha\lambda A_2^{2\alpha}} \left(\frac{x_{acc}}{x_{min}} \right)^{2\alpha a_2} \approx 1, \quad (20)$$

or

$$\frac{x_{acc}}{x_{min}} \approx \frac{\varepsilon_p^{1/2 a_2} (\eta y)^{1/(2\alpha a_2)}}{A_2^{1/a_2} [\phi(\alpha) 2^{\alpha+1}]^{1/(4\alpha a_2)}}. \quad (21)$$

It follows from equation (18) that

$$3a_2 = a_1 + 1 \quad (22)$$

Furthermore, there are two cases to be considered for the integral in equation (17) – one of which is $a_1 - 2(\alpha+1)a_2 > -1$. The integral in this case is dominated by the upper limit, and by equating the exponents of y on the two sides of the equation we find $\alpha a^2 = 1$. This together with equation (22) implies that $\alpha < 1/2$, which is not a case of interest for GRBs since the high energy spectral index for GRBs has $\alpha > 1$. The other possibility is that $a_1 - 2(\alpha+1)a_2 < -1$, and in this case pair production is dominated by photons scattered at the smallest x i.e. at x_{min} . Making use of the expression for x_{min} (eq. 21) in equation (17), and setting the exponent of y to zero results in

$$a_1 - 2a_2 = \frac{a_1 - 2a_2 + 1}{2\alpha a_2} \quad (23)$$

Solving for a_1 and a_2 from equations (22) and (23) we find

$$a_1 = 2 + 3/(2\alpha), \quad a_2 = 1 + 1/(2\alpha) \quad (24)$$

In other words the solution for \tilde{n} and γ are given by

$$\tilde{n}(x) = A_1 \left(\frac{x}{x_{acc}} \right)^{2 + \frac{3}{2\alpha}}, \quad \gamma(x) = \frac{A_2}{2} \left(\frac{x}{x_{acc}} \right)^{1 + \frac{1}{2\alpha}}, \quad (25)$$

with $A_1 \sim n \exp(\eta)$, the density at x_{acc} , and $A_2 \sim 4$. A somewhat more accurate expression for A_1 and A_2 can be obtained by combining equations (17), (18) & (24). The result in Beloborodov (2002) is a special case ($\alpha = 1$) of the solution presented here.

2.2 Spherical Expansion and Saturation of Wind Acceleration

Equations (4) and (7) were derived under the assumptions of planar geometry and stationary solution in the x -coordinate. Due to the spherical expansion, the rate of momentum deposition decreases as r^{-2} , while the rate of pair creation decreases as r^{-4} . The effect of spherical expansion is easily accounted for in a numerical treatment by decreasing the photon flux: $F(r) = F(r_{\gamma})(r/r_{\gamma})^2$, where r_{γ} is the radius at which the GRB photons were emitted, and by adjusting similarly at each timestep the laboratory frame density of the created pairs $n_{\pm}(x)$ and accelerated external electrons $n_p(x)$.

The Lorentz factor γ_{sph} and pair density \tilde{n}_{sph} at which the pair creation process saturates due to spherical expansion (*photon dilution*) can be calculated approximately as the value of these variables at the coordinate x_{sph} corresponding to a twofold increase of radius r at which the external medium entered the GRB front: $r = \int_0^{x_{sph}} dx' (1 - \beta')^{-1}$. Using equation (25), one obtains

$$x_{sph} \simeq \left[\frac{(3 + \alpha^{-1})r}{8x_{acc}} \right]^{\alpha/(1+3\alpha)} x_{acc} \quad (26)$$

and

$$\tilde{n}_{sph} \simeq A_1 \left[\frac{(3 + \alpha^{-1})r}{8x_{acc}} \right]^{\frac{4\alpha+3}{2(1+3\alpha)}} \quad (27)$$

$$\gamma_{sph} \simeq \frac{A_2}{2} \left[\frac{(3 + \alpha^{-1})r}{8x_{acc}} \right]^{\frac{1+2\alpha}{2(1+3\alpha)}} \quad (28)$$

where

$$x_{acc} \simeq \frac{1.5 \times 10^{-3} r_{15}^2 \eta}{E_{\gamma,53} \varepsilon_p^\alpha \sqrt{\phi(\alpha) 2^{1-\alpha}}} \quad (29)$$

At $x > x_{sph}$, the wind density decreases as $\tilde{n} \propto R^{-1/2} \propto x^{-2}$, where $R \sim 2\gamma_{sph}^2 x$ is the front radius corresponding to coordinate x .

The Lorentz factor of pair-wind is also limited by the non-zero transverse momentum of gamma-ray photons: the angle θ of a GRB photon w.r.t. the radial direction is $\theta = \Gamma^{-1}(r_\gamma/r)$, where Γ is the Lorentz factor of the relativistic ejecta which produced the GRB photons at r_γ . Consequently, when the pair-wind reaches the Lorentz factor $\gamma_\theta = \Gamma(r/r_\gamma)$ the photon field becomes isotropic in the frame of the moving scatterer and there is no further net transfer of momentum from photons to the wind. As shown by Beloborodov (2002), this effect yields a multiplying factor $[1 - (\gamma/\gamma_s)^4]$ in the P_{sc} term in equation (2), where $\gamma_s = \Gamma(r/r_\gamma)$. From equation (25), the acceleration saturates at coordinate $x_\theta/x_{acc} \simeq (2\Gamma r/A_2 r_\gamma)^{2\alpha/(1+2\alpha)}$, where the wind density is $\tilde{n}_\theta \simeq A_1 (2\Gamma r/A_2 r_\gamma)^{(3+4\alpha)/(1+2\alpha)}$.

Using the above equations for $r(x)$, x_{sph} , and x_θ , it can be shown that the angular dispersion of GRB photons is more important than the *photon dilution* effect (i.e. $x_\theta < x_{sph}$) at radius r less than

$$r_* \simeq \left(\frac{A_2 r_\gamma}{2\Gamma} \right)^{\frac{2(1+3\alpha)}{3+8\alpha}} \left[\frac{2.8 \times 10^{21} E_{\gamma,53} (3 + \alpha^{-1})}{T(1+z)^{-1} \eta \varepsilon_p^{-\alpha} \{\phi(\alpha) 2^{1-\alpha}\}^{-1/2}} \right]^{\frac{1+2\alpha}{3+8\alpha}} \quad (30)$$

Thus, if the GRB emission is produced in internal shocks occurring at $r_\gamma \sim 2\Gamma^2 c \delta t \sim 6 \times 10^{13} \Gamma_2^2 \delta t_{-1}$ cm, where $\delta t \sim 0.1$ s is the GRB variability timescale, the lepton density and Lorentz factor of the medium in the wake of the GRB front, at $r \lesssim 10^{14}$ cm and $\alpha = 1.5$, are

$$\tilde{n}_\theta \sim 3 \times 10^7 n \left(\frac{r_{14}}{\Gamma_2 \delta t_{-1}} \right)^3, \quad \gamma_\theta \sim 170 \frac{r_{14}}{\Gamma_2 \delta t_{-1}}. \quad (31)$$

As shown in equation (3), the acceleration of the external electrons compresses them to a density $n_{p,\theta} = 2\gamma_\theta^2 n$, therefore the pair-enrichment factor $\mu \equiv \tilde{n}/n_p$ (i.e. the number of e^- and e^+ created for each external electron) is $\mu_\theta \sim 500 r_{14}/(\Gamma_2 \delta t_{-1})$.

The medium encountered at $r > r_*$ is pair-loaded and accelerated up to the density and Lorentz factor given by equations (27) and (28). By substituting $x_{acc}(r)$ from equations (14) and (13), we obtain

$$\tilde{n}_{sph} \simeq A_1 \left[\frac{2.8 \times 10^6 (3 + \alpha^{-1}) E_{\gamma,53} \sqrt{\phi(\alpha) 2^{1-\alpha}}}{T(1+z)^{-1} r_{15} \eta \varepsilon_p^{-\alpha}} \right]^{\frac{3+4\alpha}{2+6\alpha}} \quad (32)$$

$$\gamma_{sph} \simeq \frac{A_2}{2} \left[\frac{2.8 \times 10^6 (3 + \alpha^{-1}) E_{\gamma,53} \sqrt{\phi(\alpha) 2^{1-\alpha}}}{T(1+z)^{-1} r_{15} \eta \varepsilon_p^{-\alpha}} \right]^{\frac{1+2\alpha}{2+6\alpha}}. \quad (33)$$

Note that $A_1 = \tilde{n}_{sph}(x = x_{acc}) \simeq n \exp(\eta)$, and $A_2 \sim 4$. The pair-enrichment factor $\mu_{sph} = \tilde{n}_{sph}/(2n\gamma_{sph}^2) \propto$

$(E_{\gamma,53} \varepsilon_p^\alpha / T r_{15})^{1/(2+6\alpha)}$. If $x_{sph} > \Delta$ the trailing edge of the GRB front is encountered before the wind acceleration and pair loading is saturated. This happens for electrons entering the GRB front at radii larger than

$$r_{**} \sim \frac{10^{15} (6.6 \times 10^2)^{\frac{1+3\alpha}{2+6\alpha}} [T/(1+z)]^{\frac{\alpha}{2+6\alpha}} \left[\frac{E_{\gamma,53} \varepsilon_p^\alpha}{\eta \phi(\alpha)^{-1/2}} \right]^{\frac{1+2\alpha}{2+6\alpha}}}{[2.8 \times 10^6 (3 + \alpha^{-1})]^{\frac{\alpha}{2+6\alpha}}} \text{ cm.} \quad (34)$$

In this case, substituting $x = \Delta$ in equation (25), yields

$$\tilde{n}_\Delta \simeq n \exp(\eta) \left[\frac{6.6 \times 10^2 E_{\gamma,53} \sqrt{\phi(\alpha) 2^{1-\alpha}}}{r_{15}^2 \eta \varepsilon_p^{-\alpha}} \right]^{\frac{3+4\alpha}{2\alpha}} \quad (35)$$

and

$$\gamma_\Delta \simeq \frac{A_2}{2} \left[\frac{6.6 \times 10^2 E_{\gamma,53} \sqrt{\phi(\alpha) 2^{1-\alpha}}}{r_{15}^2 \eta \varepsilon_p^{-\alpha}} \right]^{\frac{1+2\alpha}{2\alpha}} \quad (36)$$

for the maximal wind Lorentz factor and pair density, thus the pair-enrichment factor is $\mu_\Delta = \tilde{n}_\Delta / (2n\gamma_\Delta^2) \propto (\varepsilon_p^\alpha E_{\gamma,53} / r_{15}^2)^{1/2\alpha}$.

The main results of this section is that the pair creation and acceleration up to $r_{**} \sim 10^{15.3}$ cm is limited by the decrease in photon density due to spherical expansion. The pair creation for $r_{**} < r < r_{end} \sim 10^{16}$ cm continues throughout the gamma-ray pulse and the results in this regime are the same for spherical and plane parallel geometries. The medium beyond r_{end} is not affected by the passage of the GRB front.

Most of the kinetic energy of the pair-wind is acquired at $r \lesssim r_{rel}$; $r_{rel} \sim 2.6 \times 10^{16} (E_{\gamma,53} \sqrt{\phi(\alpha) 2^{1-\alpha}} \varepsilon_p^\alpha / \eta)^{1/2}$ cm, is the radius where the pair-wind Lorentz factor drop below 2. Since the pair-enrichment factor μ does not exceed m_p/m_e , the wind kinetic energy is approximately that of the entrained circumburst medium protons (or ions). Using equation (36), the wind kinetic energy is found to be

$$E_w = 4\pi n m_p c^2 \int_0^{r_{end}} r^2 \gamma_\Delta dr \lesssim 10^{47} n \varepsilon_p^{3\alpha/2} E_{\gamma,53}^{3/2} \text{ erg}, \quad (37)$$

and therefore the fraction of energy in gamma-ray pulse converted to the creation of a pair-wind is $10^{-6} n_0$. The overall wind Lorentz factor $\gamma_w = E_w / (m_w c^2) \sim 3$, where $m_w \sim (4\pi/3) r_{end}^3 n m_p$ is the wind mass.

2.3 Numerical Results

There are two factors associated with the wind spherical expansion which have been ignored in the analytical calculations presented in section §2: the spherical dilution of the incident GRB photon flux and the interactions within the pair-wind. The former has been considered in §2.2; here we note that another way in which it leads to a non-stationary $\tilde{n}(x)$ and $\gamma(x)$ is that the GRB front radius may increase significantly while a shell of external matter, undergoing acceleration and pair-enrichment, is within the front. Ignoring this effect is appropriate when the upper limit to the radius increase during the front-crossing, $2\gamma_\Delta^2 \Delta$, is less than the front radius, r , which, after using equation (36), leads to $r > 2 \times 10^{15} T_1^{0.16}$ cm for $\alpha = 1.5$, $E_\gamma = 10^{53}$ ergs, $\varepsilon_p = 1$. Collisions within the pair-wind occur because the external

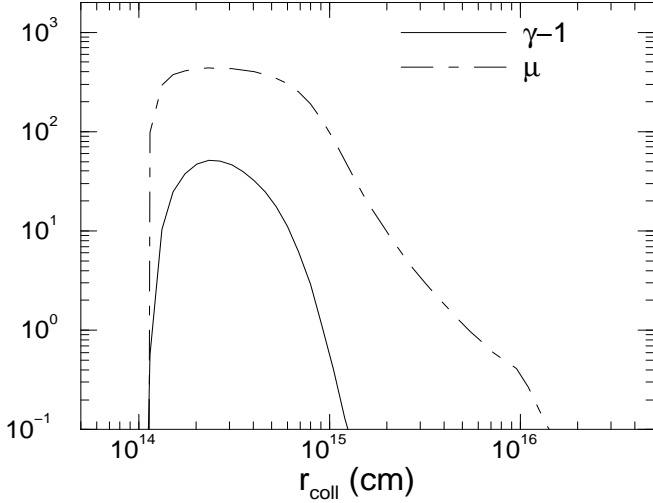


Figure 1. Wind acceleration and pair-loading for a GRB pulse of isotropic-equivalent energy $E_\gamma = 10^{53}$ erg, intrinsic duration $T = 10$ s and peak of νF_ν spectrum $\varepsilon_p = m_e c^2$, post-peak slope $\alpha = 1.5$ ($F_\nu \propto \nu^{-\alpha}$). The GRB emission is assumed to arise at $r_\gamma \lesssim 10^{14}$ cm from ejecta moving at $\Gamma = 100$. Calculations take into account the interactions within the wind, between the wind and the GRB ejecta, and the effect of spherical expansion on the incident flux and wind density. The abscissa gives the radial coordinate at which the ejecta–wind shell interactions take place.

medium entering the GRB front at smaller radius is accelerated to a higher Lorentz factor and may overtake a slower shell of external matter entering the GRB front at a larger radius. A third factor is the presence of the ejecta within the GRB pulse, which sweep-up the pair-wind and may drastically reduce the acceleration through photon-scatterings if the ejecta Lorentz factor is significantly larger than that of the wind. Thus this factor is of importance only when the lag δ between ejecta and the leading edge of the GRB front, $r/(2\Gamma^2)$, is less than the pulse width, Δ , i.e. at radii $r \lesssim 6 \times 10^{15} \Gamma^2 T_1$ cm, and only if $\Gamma \gg \gamma(\delta)$.

The effects discussed above are taken into account in the results shown in Figure 1. The external medium is discretized in shells of thickness much smaller than their radius, which entering the GRB front at $x = 0$ and are accelerated, compressed, and pair-loaded as described in §2. To include the spherical expansion, the GRB flux and the shell density are adjusted after each time-step. The progressive merging of shells (interactions within the wind) is accounted for by replacing a pair of colliding shells with one whose Lorentz factor and density are calculated from energy conservation and the jump conditions at shocks, respectively. The location of the ejecta is tracked, allowing for the accumulation of shocked wind shells and compression of the shocked ejecta.

The termination of the wind acceleration while it is still within the GRB front, due to the collision with the ejecta, is illustrated in Figure 1 by the rising part of the wind density (n_\pm) and Lorentz factor (γ_\pm) at $r \sim 10^{14}$ cm. As the ejecta lag more behind the front’s leading edge, the external medium is more accelerated and pair-loaded. The interactions within the wind and the decrease of the incident flux with radius lead to a flattening of the wind Lorentz factor at $r = 2 - 4 \times 10^{14}$ cm, followed by a decrease. The ejecta drive

the forward shock into a relativistic wind up to $r_{rel} \lesssim 10^{15}$ cm, thus the dissipation efficiency of this shock is reduced by the existence of the pair-wind up to an observer time $t_{rel} \sim (1+z)(r_{rel}/c\Gamma^2) \lesssim 10\Gamma_2^{-2}$ s. The pair production becomes negligible at $r_{pair} \sim 10^{16}$ cm, corresponding to an observer time $t_{pair} \sim 10t_{rel} \lesssim 100\Gamma_2^{-2}$ s. As shown in Figure 1, the pair enrichment factor decreases roughly as $\mu \propto r_{coll}^{-3}$ for $10^{15} < r < 10^{16}$ cm. This means that most of the radiating leptons at $r = r_{pair}$ are the pairs formed at $r < r_{pair}$ and not the electrons originally existing in the circumburst medium. Then we expect the lepton enrichment to have an effect on the afterglow emission until later than t_{pair} .

3 EARLY AFTERGLOW EMISSION

A shell of circumburst medium that enters the GRB front at radius r_{in} leaves the front at radius $r_{out} \sim r_{in} + \Delta/(1 - \beta_\pm)$, where β_\pm is the shell velocity reached when it exits the GRB front, the corresponding Lorentz factor $\gamma_\pm \equiv \gamma(x = \Delta)$ being given by equations (31), (33) or (36). The GRB ejecta collide with the pair-wind at $r_c \sim [1 + (\gamma_\pm/\Gamma)^2]r_{out}$ (assuming that $\gamma_\pm \ll \Gamma$) if the GRB ejecta are outside the front, i.e. $r_c > 2\Gamma^2\Delta$. If the GRB ejecta interact with the pair-wind while the layer is still within the GRB front, its pair-loading and Lorentz factor are lower.

In the frame of the unshocked pair-wind, the GRB ejecta move at the Lorentz factor $\gamma_r = \Gamma\gamma_\pm(1 - \beta_\pm\beta_e)$, where β_e is the ejecta velocity in the laboratory frame. Denoting by ε_e the fractional energy of the shocked wind in e^- and e^+ , the typical lepton random Lorentz factor is:

$$\gamma_p = \frac{p-2}{p-1} \varepsilon_e (\gamma_r - 1) \left(1 + \frac{n_p m_p}{\tilde{n} m_e} \right), \quad (38)$$

where p is the exponent of the power-law energy distribution $dn/\gamma_e \propto \gamma_e^{-p}$ at $\gamma_e > \gamma_p$ acquired by the leptons.

At r_c the wind density is smaller by a factor $(r_c/r_{out})^2$ than that at r_{out} . The shock compression at r_c increases the comoving density of the wind by a factor $4\gamma_r + 3$. If the magnetic field stores a fraction ε_B of the shocked wind internal energy, then the magnetic field is:

$$B^2 = 8\pi \varepsilon_B (4\gamma_r + 3) (\gamma_r - 1) (\tilde{n}_\pm m_e + n_{p,\pm} m_p) (r_{out}/r_c)^2, \quad (39)$$

where $\tilde{n}_\pm \equiv \tilde{n}(x = \Delta)$ and $n_{p,\pm} \equiv n_p(x = \Delta)$.

Figure 2 shows the evolution of the characteristic synchrotron frequency $\nu_p = (3e/16m_e c)\gamma_p^2 B\Gamma$ corresponding to a typical electron energy in the shocked wind (eq.[38]). As discussed in §2.3, the pair-wind affects the afterglow emission by reducing the energy per lepton in two ways: until $t_{rel} \lesssim 10\Gamma_2^{-2}$ s, it lowers the dissipated energy and, until some time later than $t_{pair} \lesssim 100\Gamma_2^{-2}$ s, it increases the number of particles among which this energy is shared. Both these effects lower the typical lepton Lorentz factor γ_p , leading to a softening of the afterglow emission. As the GRB front radius increases, the wind is less accelerated and pair-enriched and the afterglow spectrum hardens, its peak frequency ν_p asymptotically reaching a constant value. Note in Figure 2 that the softening of the spectrum depends on Γ , for higher initial Lorentz factor, the gap between the leading fronts of the GRB pulse and ejecta is smaller, thus the pair-wind is less accelerated and enriched before it is swept-up.

When the mass of the swept-up circumburst medium

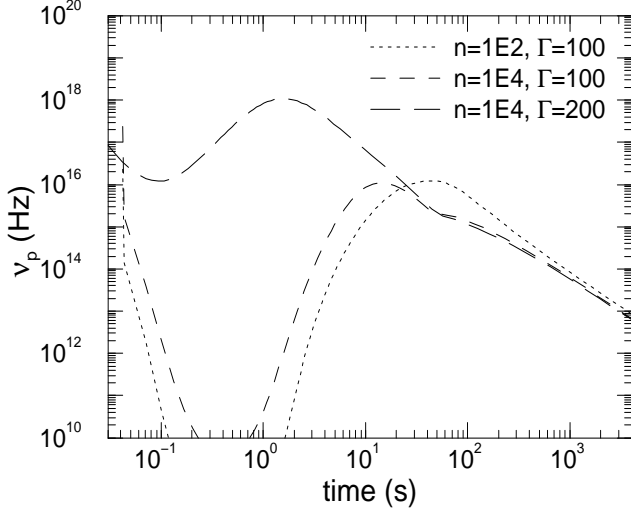


Figure 2. Evolution of the peak frequency of the synchrotron spectrum ν_p for three sets of parameters (n, Γ) (external particle density and fireball initial Lorentz factor). The burst is placed at redshift $z = 1$ (redshift), other parameters being as for Figure 1. The kinetic energy of the ejecta E_k was taken equal to E_γ (i.e. a 50% efficiency of the GRB emission was assumed). The power-law energy distribution of the shock-accelerated leptons, $dn/d\gamma_e \propto \gamma_e^{-p}$, has a total energy equal to a fraction $\varepsilon_e = 0.1$ of the post-shock energy and an index $p = 2.5$. The magnetic field energy is a fraction $\varepsilon_B = 10^{-4}$ of the internal energy. The photon arrival time is calculated for the photons moving along the line of sight toward the center of explosion. Note that the pair-wind softens the afterglow spectrum up to 10 seconds.

reaches a fraction $\sim \Gamma^{-1}$ of the ejecta mass, the fireball begins to decelerate. This happens at

$$r_{dec} \equiv \left(\frac{3E_k}{4\pi n m_p c^2 \Gamma^2} \right)^{1/3} \sim 10^{17} \left(\frac{E_{k,53}}{n_0 \Gamma_2^2} \right)^{1/3} \text{ cm}, \quad (40)$$

where E_k is the kinetic energy of the ejecta after the GRB phase, corresponding to an observer time $t_{dec} = (1+z)r_d/(\Gamma^2 c) \sim 700 (E_{k,53}/n_0)^{1/3} \Gamma_2^{-8/3}$ s. At $t > t_{dec}$, the fireball Lorentz factor is $\Gamma = [E_k/m(r)]^{1/2}$ (for adiabatic dynamics), where $m(r)$ is the mass of the energized circumburst medium. Due to the decreasing Γ , the afterglow spectrum softens again, the peak frequency evolving as

$$\nu_p(t) \sim 3 \times 10^{15} E_{k,53}^{1/2} \varepsilon_{e,-1}^2 \varepsilon_{B,-4}^{1/2} t_2^{-3/2} \text{ Hz}. \quad (41)$$

To obtain the afterglow optical light-curves, we integrate the synchrotron emission function over the electron distribution, taking into account effect of the spherical curvature of the wind surface on the photon arrival-time, photon frequency Doppler boost, and relativistic beaming. Equations (38) and (39) establish the initial distribution of the shock-accelerated pairs and the magnetic field, for the wind dynamics described in §2. We track numerically the evolution of the electron distribution (subject to radiative and adiabatic losses) in each shell of external matter, after it is accelerated and pair-loaded by the GRB front and compressed and heated by the collision with GRB ejecta. The radiative and adiabatic losses are also included in the calculation of the afterglow dynamics.

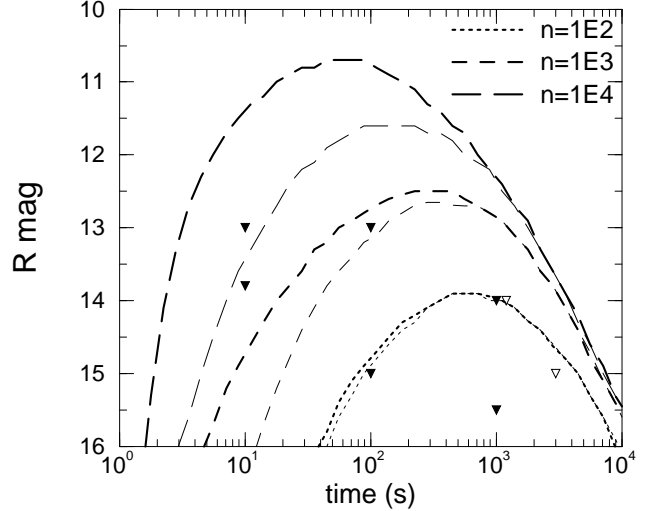


Figure 3. *Thick lines:* afterglow optical light-curves produced for various particle densities n of the circumburst medium, and for a fireball initial Lorentz factor $\Gamma = 100$. Other parameters are as for Figures 1 and 2. *Thin lines:* light-curves that would be obtained if the pair-wind were ignored. Note that the brightening of the afterglow emission during the first few minutes by the pair-wind increases with the circumburst density. Filled triangles represent upper limits obtained by ROTSE, open triangles are for LOTIS limits.

Figures 3 and 4 illustrate the effect of the pair-wind on the early optical afterglow for a few values of the circumburst medium density n and fireball initial Lorentz factor Γ . To understand better this effect, we outline first the properties of the optical light-curves expected when the radiative cooling of the γ_p -electrons and the pair-wind are ignored. Then the light-curve would peak at time t_p when ν_p passes through the optical band. Equation (41) gives that

$$t_p \sim 400 E_{k,53}^{1/3} \varepsilon_{e,-1}^{4/3} \varepsilon_{B,-4}^{1/3} \text{ s} \quad (42)$$

independent of n or Γ . The optical flux at t_p is the peak flux of the synchrotron spectrum, the corresponding optical magnitude being

$$R(t_p) = 14 - 2.5 \log(E_{k,53} n_2^{1/2} \varepsilon_{B,-4}^{1/2}), \quad (43)$$

for redshift $z = 1$. Note that $R(t_p)$ increases with the external density. The light-curves shown in Figures 3 and 4 with thin lines are consistent with the results in equations (42) and (43) for the lowest densities and Lorentz factors considered here. As the magnetic field B and typical electron Lorentz factor increase with n and Γ (eqs.[39] and [38]), the γ_p -electrons cool faster for larger n and Γ , losing their energy on a timescale shorter than the dynamical timescale ($\sim t_{dec}$). As a result, the electron distribution develops a tail at energies lower than γ_p , the peak of the synchrotron spectrum moves at a frequency below ν_p , and the optical light-curve peaks at an earlier time. The peak magnitude remains that given in equation (43).

If the early afterglow spectrum peaks above the optical domain (as is expected for values of the microphysical parameters not far from those used in eq.[41]), then the spectrum softening and increase of the number of radiating particles produced by the pair wind should brighten the afterglow

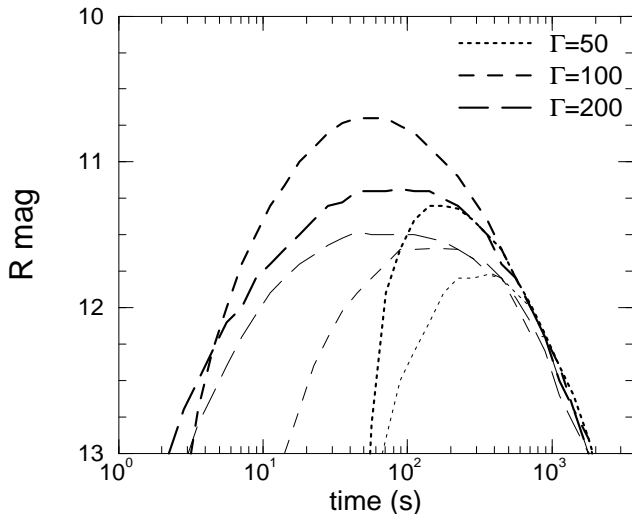


Figure 4. Same as in Figure 3, but for various ejecta Lorentz factors Γ and a fixed particle density of external medium $n = 10^4 \text{ cm}^{-3}$. Note that for $\Gamma = 100$ the brightening produced by the pair-wind is maximal. For $\Gamma \gtrsim 300$ the wind reaches only a small fraction of the maximal Lorentz factor before being swept-up by the forward shock driven by the GRB ejecta, the effect of the wind on the afterglow light-curve becoming negligible.

optical emission until a time of the order of t_{pair} . Figures 3 and 4 confirm this expectation and also show that the magnitude of the brightening induced by the pair-wind depends on the external density and ejecta initial Lorentz factor. As discussed above, a denser medium and a higher Lorentz factor lead to a faster lepton radiative cooling, which makes the optical light-curve peak at an earlier time. For the afterglow parameters considered in Figures 3 and 4, external densities larger than about $n \sim 10^3 \text{ cm}^{-3}$ lead to light-curve peak times earlier than t_{pair} . In this case, the pair-wind brightens not only the rising part of the afterglow light-curve but also its peak, the effect increasing with n . Increasing the ejecta Lorentz factor has a similar effect; however, for a larger Γ , the premature termination of the wind loading reduces the brightening produced by the pair-wind.

Summarizing the results shown in Figures 3 and 4, we can say that, without the pair-wind and for a set of representative afterglow parameters, the optical afterglow peak should be brighter than $R = 13$ for $n \gtrsim 10^3 \text{ cm}^{-3}$, should increase by one magnitude for an ten-fold increase in the external density, but this peak should occur earlier than 100 seconds if $n \gtrsim 10^4 \text{ cm}^{-3}$. Further, for $\Gamma \lesssim 200$, the pair-wind brightens the optical afterglow peak of the optical afterglow by half of a magnitude for $n = 10^3 \text{ cm}^{-3}$ and by 1 magnitude for $n = 10^4 \text{ cm}^{-3}$; however, for $\Gamma \gtrsim 200$, the effect of the pair-wind is reduced.

For the canonical afterglows parameters given in Figure 2 and $n \sim 10^4 \text{ cm}^{-3}$, the optical afterglow shown in Figures 3 is brighter than the upper limit $R \gtrsim 13$ at $t = 10 \text{ s}$ set by the ROTSE experiment (Akerlof et al. 2000, Kehoe et al. 2001) for the prompt optical emission of two GRBs; however, a lower density or a higher Lorentz factor (suppressing the pair-wind brightening), would explain the non-detections. Similarly, the upper limits ranging from $R = 13$ to $R = 15$, obtained by ROTSE at $t = 100 \text{ s}$ for three bursts, require

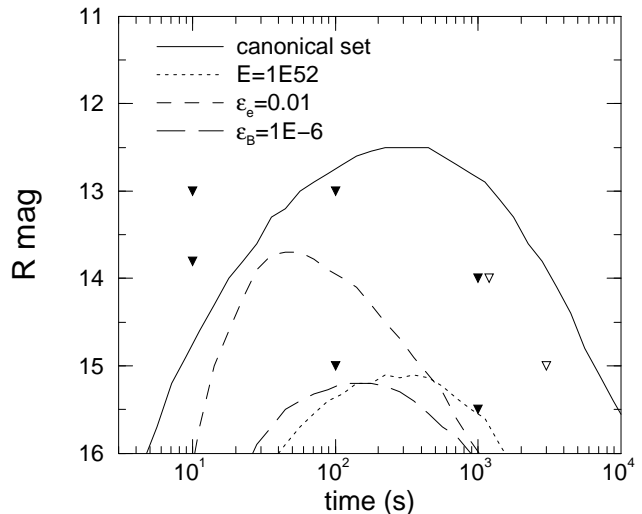


Figure 5. Effect of the burst energy, electron, and magnetic field parameter on the afterglow optical emission. The canonical set of parameters is: $n = 10^3 \text{ cm}^{-3}$, $\Gamma = 100$, $E_k = E_\gamma = 10^{53} \text{ erg}$, $z = 1$, $T = 20 \text{ s}$, $\varepsilon_p = m_e c^2$, $\alpha = 1.5$, $\varepsilon_e = 0.1$, $\varepsilon_B = 10^{-4}$, $p = 2.5$. Varying the burst duration, the peak energy of the GRB spectrum, or its slope has little effect on the resulting afterglow light-curve.

that $n \lesssim 10^3 \text{ cm}^{-3}$ and $n \lesssim 10^2 \text{ cm}^{-3}$, respectively, the pair-wind having a small effect at such times and for such densities. Finally, $n < 10^2 \text{ cm}^{-3}$ is required by the upper limits ranging from $R = 14$ to $R = 16$ set at $t = 10^3 \text{ s}$ by ROTSE for five bursts (see also Rykoff et al. 2002) and by $R(t > 1200 \text{ s}) > 14$ and $R(t < 3000 \text{ s}) > 15$ obtained by LOTIS for GRBs 971227 and 010921, respectively (Williams et al. 1999, Park et al. 2002).

The above comparison between expectations and observations for the early afterglow emission suggest that the circumburst density does not exceed $n = 10^2 - 10^3 \text{ cm}^{-3}$, unless the microphysical parameters ε_B and ε_e and the kinetic energy E_k have lower values than considered for Figures 3 and 4. The effect of these parameters is illustrated in Figure 5 for $n = 10^3 \text{ cm}^{-3}$ and $\Gamma = 100$. A kinetic energy E_k lower than 10^{52} ergs or magnetic field parameter ε_B below 10^{-6} yield an early afterglow emission too dim to have been detected with the past capabilities of ROTSE or LOTIS, but within their reach in the future. For a lower electron energy, past detections were more difficult, but not impossible. We note that such low values for E_k and the γ -ray output energy E_γ obtained by Bloom, Frail & Sari (2001) for bursts with known redshifts, ranging from $10^{51.5}$ to $10^{54.5} \text{ erg}$, would imply high burst efficiencies. Furthermore, the above low values for ε_e and ε_B are below the values $\varepsilon_e > 0.1$ and $\varepsilon_B > 10^{-4}$ determined by Panaitescu & Kumar (2002) from fits to the 0.5–100 days broadband afterglow emission of several GRB afterglows.

Therefore, barring a substantial increase of the ε_e and ε_B parameters from $10^2 - 10^3 \text{ s}$ to 10^5 s after the burst, the non-detections by LOTIS and ROTSE of GRB optical counterparts brighter than $R = 13-16$ at $t < 3 \times 10^3 \text{ s}$ imply that the medium surrounding the GRB source is less dense than $n = 100 \text{ cm}^{-3}$ up to a distance $r \sim 0.01 \text{ pc}$.

Figures 6 and 7 present the afterglow light-curves ex-

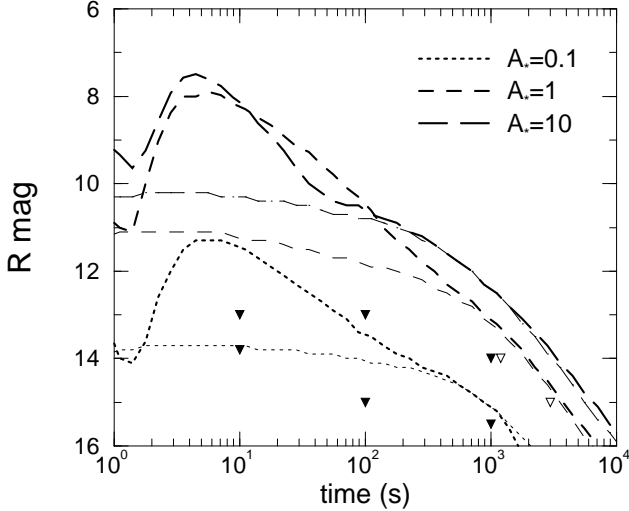


Figure 6. Afterglow light-curves for the same parameters as in Figures 1 and 2, but for an external medium of density $n = Ar^{-2}$, as expected if the GRB progenitor is a massive star. The legend gives the constant A divided by that corresponding to a mass-loss rate of $10^{-5} M_{\odot}/\text{yr}$ and a stellar wind speed of 10^3 km/s. Thick lines are for the afterglow light-curve calculations including the pair-wind, while thin lines show light-curves obtained if the pair-wind were ignored. Note that the pair-wind brightens the afterglow emission during the first minute by up to 3 magnitudes, its effect disappearing after the second minute. at the peak.

pected when the circumburst medium is a stellar wind of density profile $n = Ar^{-2}$ ejected by the GRB progenitor, as expected in the hypernova scenario. In contrast with the homogeneous medium case considered in Figures 3 and 4, the brightening produced by the pair wind is stronger (2–3 mags), occurs earlier, and has a weak dependence on the normalization constant A (i.e. the wind density), but a stronger dependence on the ejecta Lorentz factor. For the canonical burst parameters used here, optical afterglows brighter than some of the ROTSE and LOTIS limits are obtained even for tenuous stellar winds corresponding to a mass-loss rate to wind speed ratio of $10^{-6} M_{\odot}/\text{yr}/(10^3 \text{ km/s})$.

4 CONCLUSIONS

Assuming that GRBs are produced by internal shocks at $10^{13} - 10^{14}$ cm, a small fraction of the gamma-ray photons is converted into electron-positron pairs at a distance of less than $r_{\text{pair}} = 10^{16}$ cm from the center of explosion. The fractional energy carried away by this pair-wind is $\sim 10^{-6}n$, where n is the particle density in cm^{-3} of the unperturbed, circumburst medium. The number of pairs created per external electron is of order a few hundred and the average Lorentz factor of the pairs is a few.

For plausible values of the fireball kinetic energy, electron and magnetic field parameters in the shocked circumburst medium, and for an external density $n = 100 \text{ cm}^{-3}$, the optical afterglow from the forward shock peaks around 10 minutes from the burst (when the peak of the synchrotron spectrum reaches the optical domain) and at magnitude $R \sim 14$ (Figure 3). For a tenfold increase in the density,

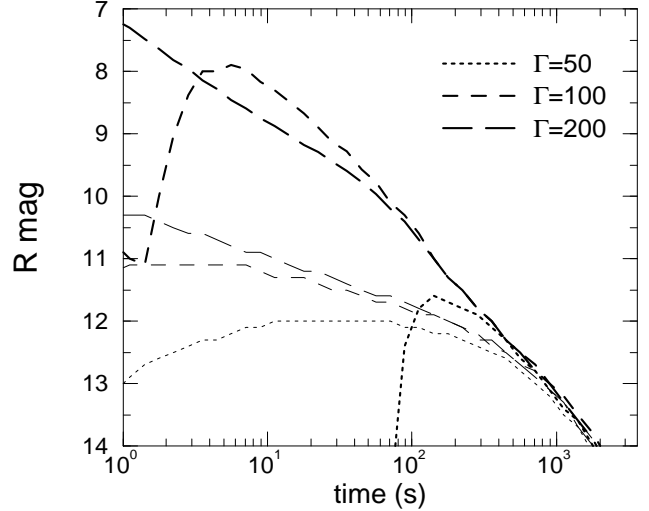


Figure 7. Afterglow light-curves for the parameters given in Figure 6, for the ejecta Lorentz factors given in legend and a stellar wind with $A_{*} = 1$. For $\Gamma = 50$ the pair-wind reaches initially a Lorentz factor γ_{\pm} larger than that of the GRB ejecta and a gap develops between them, the afterglow emission starting when γ_{\pm} has fallen below Γ and the ejecta sweep-up the pair-wind. As for Figure 6, the effect of the pair-wind on the afterglow emission subsides after a couple of minutes.

the peak brightens by one magnitude (eq.[43]) and occurs earlier due to the electron cooling.

By softening the afterglow spectrum and by increasing the number of radiating particles, the pair-wind brightens the rise of the optical light-curve. For densities higher than $n \sim 10^3 \text{ cm}^{-3}$ the peak optical emission occurs at radii where the pair production is significant, leading to a brightening of the optical peak emission (Figure 3) if the ejecta Lorentz factor is less than $\lesssim 300$ (Figure 4). A higher Lorentz factor suppresses the pair-wind acceleration/enrichment and its brightening of the afterglow emission until $t_{\text{pair}} = (1+z)r_{\text{pair}}/(c\Gamma^2) \sim 10(\Gamma/300)^{-2}$ s, but leaves unaltered the afterglow emission at later times, past the deceleration timescale.

For conservative values of the afterglow kinetic energy and electron/magnetic field parameters, the upper limits set by ROTSE and LOTIS on the prompt optical emission from several GRBs at $10^2 - 10^3$ s, ranging from 13 to 16 mag, require that the density of the circumburst medium within 0.01 pc of the GRB progenitor is less than 100 cm^{-3} . This limit is consistent with the typical densities of $0.1 - 30 \text{ cm}^{-3}$ inferred at $r > 10^{17}$ cm from fits to the broadband emission of several GRB afterglows (e.g. Panaitescu & Kumar 2002). Moreover, our results show that a wind-like medium around the GRB progenitor, corresponding to a mass-loss to wind speed ratio above $10^{-5} M_{\odot}/\text{yr}/(10^3 \text{ km/s})$ yields optical counterparts brighter than $R = 13$ up to almost 10^3 s. Thus, the wind of a Wolf-Rayet star is too dense and incompatible with the ROTSE and LOTIS upper limits.

Figures 3, 4, 6, and 7 show that the brightening of the pair-wind of the early afterglow emission is much more prominent for a wind-like external medium. This feature is present within the first 100 seconds of the optical afterglow

and provides a test for the type of circumburst environment, using future Swift observations.

For $n \gtrsim 10^6 \text{ cm}^{-3}$ all photons with energy above the threshold for e^\pm production are transformed into pairs and the GRB spectrum is severely modified. In this case the pair-wind becomes optically thick to Thomson scattering and the burst may not be detectable. However, an optical counterpart resulting from the interaction of the ejecta with the pair-wind would be very bright ($R \sim 10$), unless it is attenuated by the dust within the dense medium. Such flashes, if produced, would be missed by ROTSE and LOTIS, in the absence of the GRB emission.

ACKNOWLEDGMENTS

We acknowledge many interesting discussions with Bohdan Paczyński, who suggested that we investigate the effect of pair-wind on GRB optical afterglows. We are indebted to the referee, Andrei Beloborodov, for a number of helpful suggestions that have improved the paper significantly.

REFERENCES

- Akerlof, C. et al. 2000, ApJ, 532, L25
Beloborodov, A. 2002, ApJ, 565, 808
Bloom, J., Frail, D. & Sari, R. 2001, AJ, 121, 2879
Kehoe, P. et al. 2001, ApJ, 554, L159
Mészáros, P., Ramirez-Ruiz, E., & Rees, M.J. 2001, ApJ, 554, 660
Park, H. et al. 2002, ApJ, 571, L131
Panaitescu, A. & Kumar, P. 2002, ApJ, 571, 779
Preece, R., Briggs, M., Mallozzi, R., Pendleton, G., & Paciesas, W. 2000, ApJS, 129, 19
Rykoff, E. et al. 2002, GCN #1480
Svensson, R. 1987, MNRAS 227, 403
Thompson, C. & Madau, P. 2000, ApJ, 538, 105
Williams, G. et al. 1999, ApJ, 519, L25